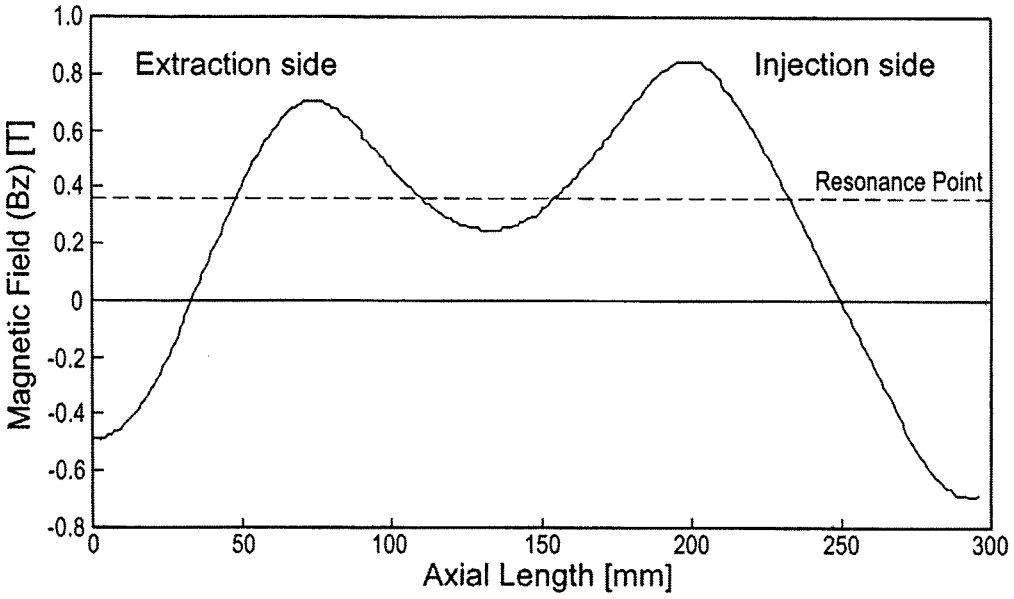

Figure 3. Distribution of magnetic field strength in the axial direction.

cross-sectional view of the ECRIS, the first chamber and the extraction chamber. The magnetic mirror field is produced by four ring magnets. A hexapole magnet is inserted into the center of the ring magnets and a magnetic field direction of the hexapole magnet is perpendicular to a magnetic field direction of the ring magnets. The magnetic field distribution in the axial direction is shown in Figure 3. When the strengths of the axial confinement magnetic field by the ring magnets and the radial confinement magnetic field by the hexapole magnet are high, the confinement of electrons is enhanced and stable plasma that contributes to the measurement precision of the mass spectrometer is generated. In order to improve the confinement of electrons by the applied magnetic field and to generate stable ECR plasma, the ECRIS has a magnetic field higher than that produced by all types of permanent magnets of typical ECRISs using high frequency of 10 GHz. As we intend to achieve a broad charge state distribution, the intensity of the magnetic field on the extraction side is slightly increased.[6] Although the total and peak ion currents tend to decrease, their values are sufficient for the analysis of the distribution.

The main specifications of the ECRIS are listed in Table 1. To prevent the demagnetization of the permanent magnets by the heat from the ECR plasma, the plasma chamber is cooled by pure water at approximately 20°C. The minimum permeance coefficient for the entire magnetic circuit is −0.275. The heatproof temperature for the permissible demagnetization range of 1% is approximately 50°C because the magnetic material of the hexapole magnet is N39UH. The first chamber, plasma chamber and extraction chamber are connected by metal seals. All the flanges of the first and extraction chambers are sealed with metal gaskets and the interiors of all the chambers are electrolytically polished. The vacuum level reaches 1×10^{-7} Pa due to sealing and polishing.

The extraction electrode, which is connected to an Einzel lens electrode, can be moved along the beam direction in the extraction chamber. The voltage of the Einzel lens was set at the value at which the ion currents in the Faraday cup were maximum. It was decided that the position of the lens should be at the position at which the peak shape of the mass spectrum improved. The space-charge effect was minimized by maintaining the value of the total beam current below a few hundred microamperes. The diameters of the holes of both

Table 1. Specifications of the ECRIS.

Mirror magnet	
Material	NdFeB
Maximum field strength	
Injection side	0.85 T
Extraction side	0.70 T
Minimum field strength	0.25 T
Hexapole magnet	
Maximum field strength	1.48 T
Chamber surface	0.85 T
Length	120 mm
Inner diameter	62 mm
Plasma chamber	
Internal diameter	50 mm
Length	160 mm
High frequency	
Frequency	10 GHz
Maximum power (TWTA)	650 W
Wave guide	WR-75

the plasma electrode and the extraction electrode were 6 mm. The distance between the two electrodes was 21 mm. The calculated space-charge limit was almost 0.4 mA. In view of the drain current from the high-voltage power supply, the extracted total ion current was 0.18 mA or less.

In the case of our dipole magnet, the positions of the object and image focal points are at the same distances along the axis of symmetry of the magnet. The positions are 1400 mm from the entrance (or exit) of the magnet. However, with regard to the beam transport, the starting point is not clear in the case of the ECRIS. Because the spatial distribution of the extracted ions depends on the mass-to-charge ratio, the main slit behind the extraction electrode could not be used. Hence, in order to determine the location at which the resolution is the highest, the ion source component and the detection component were mounted on a slide rail, and they could, therefore, be moved linearly and smoothly.

We used a traveling-wave-tube amplifier (TWTA) manufactured by NEC Microwave Tube, Ltd. It produces a high frequency of 10 GHz and a maximum output power of 650 W. The power of the high frequency can be changed continuously. Microwaves are transmitted to the plasma chamber by a waveguide; the waveguide comprises a DC break block for isolation from the high extraction voltage and an EH tuner for high frequency matching. A vacuum is maintained in the chamber by means of a quartz pressure window developed by CPI/MPP. The flange with the pressure window is attached to the injection waveguide by using a metal O-ring. Therefore, the outgas produced by the heat by high frequency power loss in the window is minimized.

Analyzing magnet

A dipole magnet with a C-type yoke is used to analyze the multi-charged ions extracted from the ECRIS. Table 2 lists the main specifications of the analyzing magnet. For obtaining magnetic field measurements, a hall probe is installed at the center of the outer surface of the inner curve of the flight chamber. We used an Agilent 6691A power supply, which produces low ripple and noise, for the magnetic coil. The measurement accuracy of the *m/z* value can be improved by controlling the magnetic field measured by the hall probe and the current monitor output of the power supply.

Table 2. Specifications of the analyzing magnet.

Radius of curvature	700 mm
Bending angle	90°
Pole gap	73 mm
Flight chamber gap	60.5 mm
Flight chamber width	180 mm
Edge angle	26.57°
Magnetomotive force	19200 AT
Maximum coil current	200 A
Maximum magnetic field	0.32 T

Detection system

Usually, the intensity of the ion current from the ECRIS is significantly higher than that of the current from other mass spectrometers. For example, ion beams of multi-charged Ar greater than 10 μA can be obtained by optimizing the high frequency power and the gas pressure. However, in this system, an injection slit cannot be used downstream of the extraction electrode because the space distribution of the ion beam extracted from an ECR ion source depends on *m/z*. Therefore, when a quantity and a shape of the ion beam is changed before reaching the dipole magnet by using a main slit, etc., it becomes the cause of a mass discrimination effect. Since a thin slit, etc., is not used, the ion current measured with a detection system is large in comparison with other analytical systems. Therefore, a new Faraday cup (FC) that was suitable for small and large currents with low noise was developed. The FC and a picoammeter are connected by a lead-through with double shields, triaxial cables and triaxial connectors. The FC and slit system are insulated from the beam line and trestle in order to protect them from the effect of the noise produced by the electrical discharge of the ion source and vacuum systems on the beam duct. The dark current was measured to be approximately 200 fA. There was no difference between the dark current values measured with and without the operation of the ion source. Corrector slits that can be moved in the up, down, left and right directions were installed in front of the FC.

Measurement of noble gases

By using high-purity Ar and Kr gases, each low-charged ion was measured for performance evaluation as the first step in this system. Table 3 shows the main operating parameters of the ECRIS for producing Ar and Kr ions.

Figure 4 shows the typical spectrum of the charge-state distribution of the Ar ions. The spectra (ion current as a function of the analyzing magnet current) shown in Figures

Table 3. Main parameters of the ECRIS for noble gas measurements.

	Ar	Kr
Extraction voltage	10.00 kV	10.00 kV
Drain current	0.21 mA	0.28 mA
Einzel lens voltage	2 kV	2.6 kV
High frequency power	100 W	106 W
High frequency reflection power	3 W	12 W
Gas pressure	5.5e–5 Pa	4.0e–5 Pa

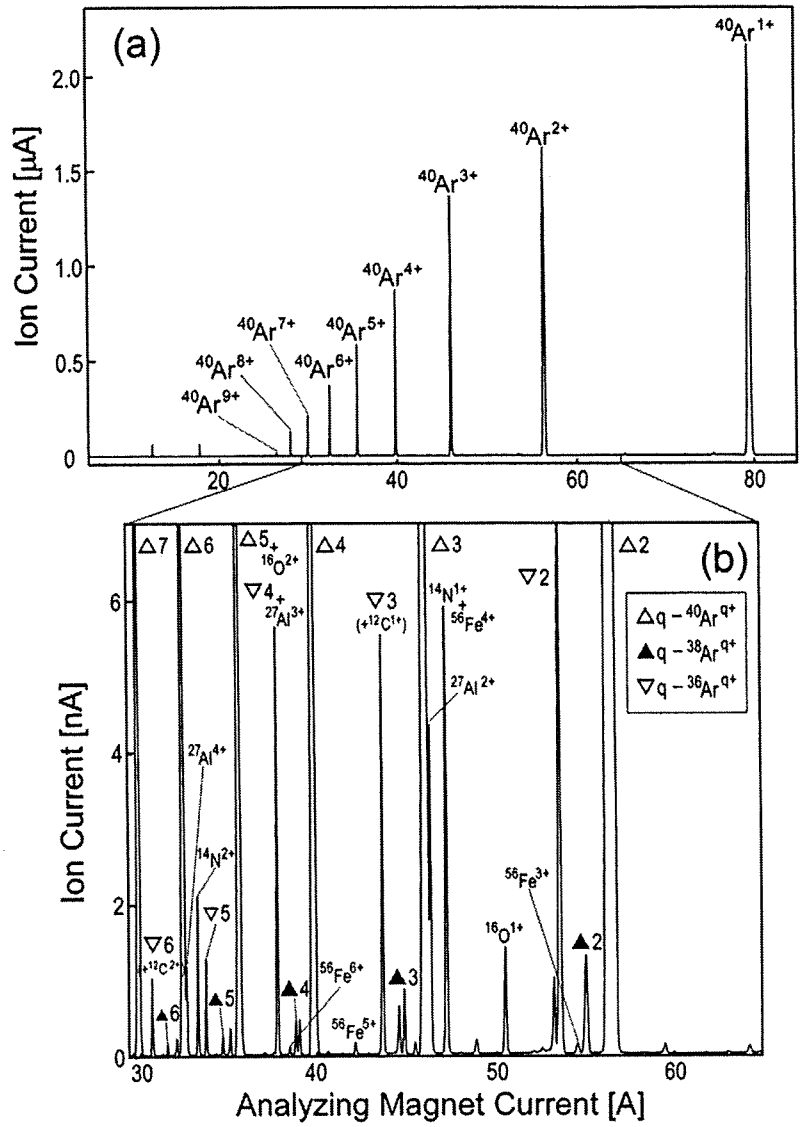

Figure 4. Ion current as a function of the analyzing magnet current. Typical spectrum of the charge-state distribution of Ar ions. Both (a) and (b) were obtained by performing the measurement once.

4(a) and 4(b) were obtained in a single measurement. Subsequently, the spectrum of the charge-state distribution of Ar was measured 10 times in 1.5 h without changing the parameters of the ion source. The duration of each measurement was approximately 5 min and the speed for scanning the magnet was approximately 0.3 As^{-1}. In Table 4, the stability level of the ion current from 1+ to 8+ is shown as the standard deviation of the values obtained after performing the measurements 10 times for approximately 90 min. For the 3+ spectra of ^{40}Ar, the mass-to-charge ratio value of $^{40}Ar^{3+}$ is close to that of $^{27}Al^{2+}$. It was not possible to separate the values in the scale range of the horizontal and vertical

Table 4. Long-time (90 min) stability of Ar ion current from the ECRIS.

Charge state	1	2	3	4	5	6	7	8
Ion current[a] (nA)	1922	1638	1370	720	412	258	158	116
Stability[b] (nA)	9.8	9.3	29	18	13.3	11.5	8.8	6.8
Ratio (%)	0.51	0.57	2.2	2.5	3.3	4.6	5.6	5.9

[a]Average value obtained by measuring ten times
[b]Standard deviation

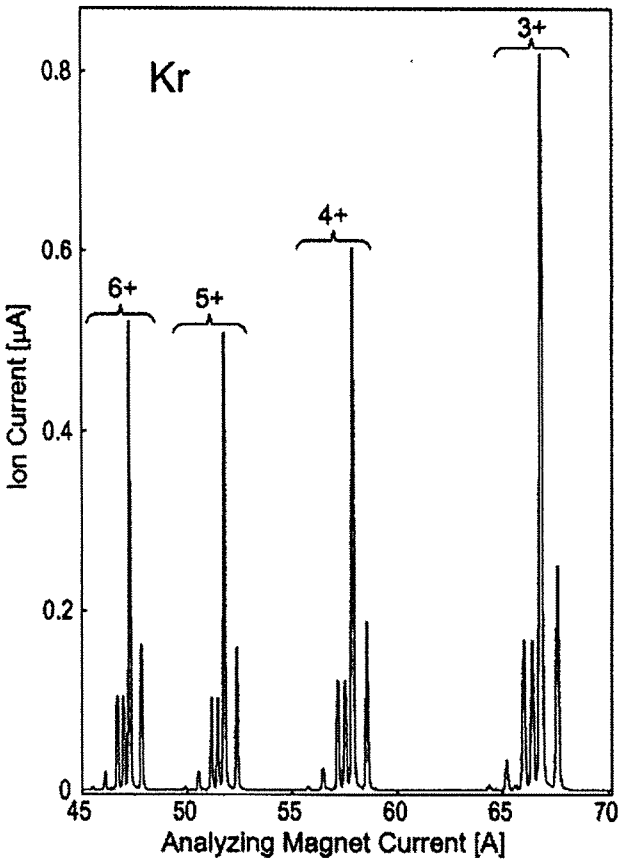

Figure 5. Kr ion current as a function of the analyzing magnet current. Typical spectrum of the charge-state distribution of Kr ions.

axis of Figure 4(a). Hence, it was considered that these values changed due to the overlapping of the two spectra. The two spectra were separated, as shown in Figure 4(b), by doubling the scale of the spectra shown in Figure 4(a). The inner cylinder was made of pure Al in order to protect the plasma chamber from being heated up by the spattering of high-energy electrons in the ECR plasma. Aluminum ions are generated from this cylinder. The spectrum of Fe ions was also observed in Figure 4(b) due to similar reasons. In this case, the plasma electrode was made of stainless steel 316L. It appears that the problem of overlap can be solved by changing the materials when it becomes difficult to measure the spectra. Moreover, if a clean environment is necessary for the plasma chamber, it is preferable to use a quartz tube.[7]

With the exception of ^{38}Ar, stable elements with mass numbers of 38 do not exist. In this measurement, if there is no element whose mass number is a multiple and a common divisor of 38 and the isotope of Ar does not occur, the ion currents for ^{36}Ar and ^{40}Ar are calculated from the ion current of ^{38}Ar accurately. In the charge distribution, the part of the $^{27}Al^{3+}$ spectrum that overlaps with the $^{36}Ar^{4+}$ spectrum can be determined by the subtraction of a peak height of the $^{36}Ar^{4+}$ spectrum. The peak height of the $^{36}Ar^{4+}$ spectrum is calculated from the isotope abundance of argon when there are no scientific abnormalities in the isotope ratio of argon. This indicated that the problem of overlap such as that observed in the spectra of isobars can be solved without any significant improvement in the mass resolution by using the charge state distribution and isotope ratio.

Figure 5 shows the typical spectrum of the charge-state distribution of Kr ions. By using the spectrum (Kr ion current as a function of the analyzing magnet current) obtained by a single measurement, the isotope ratio of Kr was obtained from the results of the charge states of the 3+, 4+, 5+ and 6+ spectra. This was compared with the isotope ratio in a terrestrial atmosphere[8] and is shown in Table 5. The measurement of the spectrum was carried out once. This spectrum was recorded with an X–Y pen recorder. The standard deviation for measuring the isotope of each charge number with a vernier micrometer was very small. The error margin in the measurement accuracy (+/−0.05 mm) of the vernier micrometer was larger than the standard deviation. The measurement by the vernier micrometer was performed once. With regard to the error margin given in Table 5, the error in the

Table 5. Isotopic ratio of Kr in comparison with that in the terrestrial atmosphere.

	$^{78}Kr/^{84}Kr$	$^{80}Kr/^{84}Kr$	$^{82}Kr/^{84}Kr$	$^{83}Kr/^{84}Kr$	$^{86}Kr/^{84}Kr$
ECRIS mass spectrometer	6.1e–3	0.0397	0.202	0.200	0.308
+/–	0.4e–3	0.0004	0.001	0.001	0.001
Terrestrial atmosphere[a]	6.10e–3	0.0396	0.2022	0.2016	0.3055
+/–	0.03e–3	0.0002	0.0005	0.0005	0.0007

[a]See Reference 8. All ratios were normalized by ^{84}Kr. The error margin was simply calculated from the percent ratio of each error margin.

Table 6. Ingredients of the standard gas chosen from noble gases.

Ingredient	He	Ne	Ar	Kr	Xe
Purity	99.9995%	99.99%	99.99%	99.99%	99.99%
Amount	Balance	101 ppm	101 ppm	102 ppm	102 ppm

Table 7. Evaluation of the precision of isotopic analysis of noble gas compounds. Upper subscript "m" represents atomic mass numbers to the line. "*M/z*" is mass-to-charge ratio.

M/z	124	126	128	129	130	131	132	136			
$^{m}Xe^{+}/^{134}Xe^{+}$	124	126	128	129	130	131	132	136			
	0.00910	0.00875	0.188	2.540	0.3912	2.049	2.575	0.8471			
err.(+/−)	0.00005	0.00004	0.003	0.008	0.0032	0.007	0.008	0.0039			
M/z	78	80	82	84	86						
$^{m}Kr^{+}/^{83}Kr^{+}$	78	80	82	84	86						
	0.034	0.252	1.013	4.997	1.477						
err.(+/−)	0.001	0.002	0.007	0.025	0.009						
M/z	39	40	41	41.3	42	42.6	43	43.3	43.6	44	45.3
$^{m}Kr^{2+}/^{83}Kr^{2+}$	78	80	82		84		86				
	0.078	*24.7*	1.11		4.86		1.56				
err.(+/−)	—	—	0.07		0.02		0.01				
$^{m}Xe^{3+}/^{134}Xe^{3+}$				124	126	128	129	130	131	132	136
				—	—	0.16	2.603	0.370	2.047	*3.364*	0.8309
err.(+/−)				—	—	0.01	0.002	0.005	0.013	—	0.0076
Terrestrial atmosphere											
$^{m}Xe/^{134}Xe^{a}$	124	126	128	129	130	131	132	136			
	0.009096	0.008477	0.1834	2.534	0.3896	2.035	2.577	0.8500			
err. (+/−)	0.000055	0.000055	0.0007	0.006	0.0011		0.005	0.0023			
$^{m}Kr/^{83}Kr^{b}$	78	80	82	84	86						
	0.0303	0.196	1.003	4.960	1.515						
err.(+/−)	0.0001	0.001	0.002	0.011	0.003						

[a]See Reference 11. All ratios were normalized by ^{134}Xe. The error margin was simply calculated from the percent ratio of each error margin.

[b]See Reference 8. All ratios were normalized by ^{83}Kr. The error margin was simply calculated from the percent ratio of each error margin.

measurements performed with the vernier micrometer was used. The results obtained by using the charge-state distribution in the measurement performed once with high precision are in good agreement with the reference data. The error limits are estimated from the precision of the measurements of the peak height with a vernier micrometer. It should be noted that the above-mentioned results are obtained without any regular alignment of the ion source, the FC systems and beam optics.

From our preliminary data, we have not identified any apparent isotope effects or fractionations that depend on the mass. Kawai *et al.* have reported such isotope effects (mass discrimination effect) for nitrogen in an ECRIS.[9] They have explained the isotope anomaly (mass discrimination) based on the ion Landau damping due to the influence of low-frequency noise. In relation to the ion Landau damping, the possibility of mass discrimination due to the effect of gas mixing might have to be considered. The gas mixing method has been researched and used widely in the ECRISs of many accelerator facilities where an intense beam of highly-charged ions is required. The beam intensities of the highly-charged

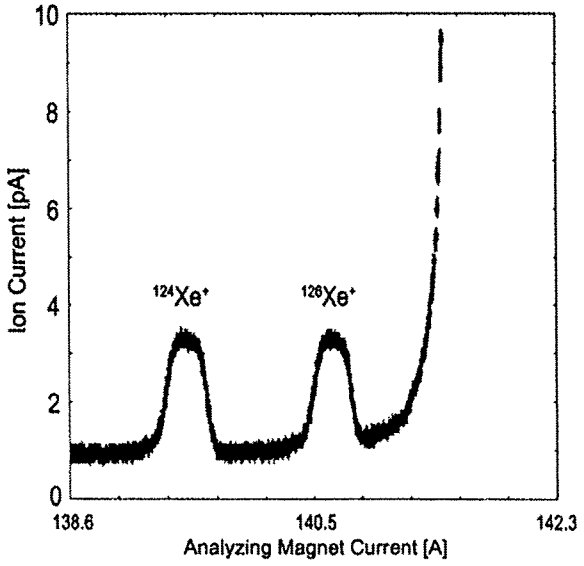

Figure 6. Spectrum of 1+charge state of ^{124}Xe and ^{126}Xe; the relative abundances of these elements are 0.10% and 0.09%, respectively.

ions of Ar were (or were not) altered by mixing gases such as H, He, $^{14,15}N$ and $^{16,18}O$. It is thought that this effect influences the charge-state distribution through ion cooling.[10] Depending on the selected gas, the influence of ion cooling might alter the isotope ratio of a low-charge state. This influence on the isotope ratio of low-charge states (2+, 3+, 4+, ...) has not been systematically examined in the mixing of metal elements and various gases. In our isotope measurements of pure Kr, a systematic isotope anomaly (mass discrimination) was not observed within the measurement precision. In ECR plasma, a careful observation of the isotope anomaly (mass discrimination) in the low-charge state should be conducted in the future.

Preliminary measurements with a standard gas

For the demonstration of elemental analysis employing low charge-state distribution, a standard gas chosen from the noble gases was measured by this system. The ingredients of the standard gas are listed in Table 6. Eight spectra, which appropriately changed the range of the mass-to-charge ratio values and the current meter, were obtained. The analytical values in Table 7 were derived from the results of the single measurement of peak heights in the above-mentioned eight spectra with the vernier micrometer. Figure 6 shows the spectra of $^{124}Xe^+$ and $^{126}Xe^+$. The provisional sensitivity in this preliminary measurement was 0.1 ppm as observed in Figure 6. In the measurement employing this standard gas, Kr^+ and Xe^+ do not have the same mass numbers as those of the other elements. Therefore, Kr^+ and Xe^+ in Table 7 are the values pertaining only to Kr and Xe, respectively. It could be inferred that there was no serious isotope anomaly (or mass discrimination) in Kr and Xe from these values. Because it is the analytical value from only one charge state, the error margin is large in comparison with that of Kr in Table 5. The peaks of $^{126,129}Xe^{3+}$ overlapped with the peaks of $^{84,86}Kr^{2+}$, respectively. The isotope ratio of $^{129}Xe^{3+}$ was calculated by using the isotope abundance of $^{86}Kr^{2+}$. On the contrary, the isotope ratios of $^{84,86}Kr^{2+}$ in the table were calculated by using the isotope abundances of $^{126,129}Xe^{3+}$, respectively. Accurate isotope ratios of $^{84,86}Kr^{2+}$ and $^{129}Xe^{3+}$ were derived by this method. In the isotope ratio of $^{80}Kr^{2+}$, $^{40}Ar^+$ was mainly included. Ultratrace elements of Ag, Cd and Sn were observed in this experiment. The presence of these elements is thought to be due to the use of silver brazing filler metals in order to connect the square flanges of the waveguide, which is used to introduce the high frequency into the system. The isotope ratios of $^{78}Kr^{2+}$ and Ar could not be calculated with good precision because of this contamination. If these contaminations pose acute problems, the problems are solved by using a waveguide that does not use silver brazing. Further, in the isotope ratio of $^{132}Xe^{3+}$, CO_2 was possibly included. Concerning the origin of CO_2, the background of the system and/or the contaminations in the standard gas were enumerated. However, in both cases, the amounts obtained were inconsistent. Hence, it will be necessary to investigate the origin of CO_2 in detail in the future.

The measurement of each of the above-mentioned spectra and the analysis with the vernier micrometer was performed only once. If measurements are carried out for the flat top of the peaks and a multi-collector and a data-taking system with statistical measurements are employed, it is clear that the measurement precision and the detection sensitivity can be significantly improved.

Consideration of sample form

In this measurement, a gaseous sample was introduced into the ECRIS. The gaseous sample is suitable for the ECRIS because it can control a very small amount of gas in the plasma chamber. In the case of solid samples, particularly in metal ion production, many production techniques such as the insertion method, metal ions from volatile compounds (MIVOC) method, micro-oven method, IH oven method and the spatter method have been developed and improved by many researchers in the field of ECRIS research.[5] However, the direct ionization of a liquid sample in the ECRIS has not been investigated extensively because it is difficult to maintain a steady supply into the high vacuum chamber. Usually, ECR plasma is generated in the vacuum range from 10^{-2} to 10^{-5} Pa. In this range, it is possible to control the stable feeding and the evaporation of gas and solid samples. Liquid samples are primarily used in the field of elemental analysis. Currently, we are developing a method for the introduction of a liquid sample into the ECRIS.

Conclusions

Precise measurements are performed on Ar and Kr gases by using an ECRIS that has been customized for elemental analysis. The measurement results of Ar indicate that long-time stable ionization can be achieved without operating the ECRIS. It means that ECR plasma is stable for a long time, without readjusting the ion source parameter. The measurement results of Kr reveal that the elemental analysis system equipped with this ion source can be successfully used for isotope analysis. In this measurement, a systematic isotope anomaly (or mass discrimination) is not observed. Furthermore, in the measurement of the noble gas compound, we indicated the possibility of isotopic analysis by using the ECR ion source and a low-charge state. In the future, the isotope anomaly (mass discrimination effect) will be investigated in detail by using this analysis system, which can perform precise measurements. In order to increase the profitability of this system, it is crucial to develop a method for introducing a liquid sample in the ECRIS. The ECRIS can be expected to show a high performance for most of the elements of the periodic table and to be applicable to several scientific

fields such as environmental, material, geochemical and bioanalytical chemistry that require isotopic and elemental analyses.

Acknowledgments

We are grateful to Mr M. Hemmi for assisting us with the microwave technique, electronics and ion current measurement. This study was supported by a Grant-in-Aid from the President's Discretionary Fund, RIKEN and a Grant-in-Aid for Scientific Research (KAKENHI:19540515).

References

1. F. Adams, R. Gijbels and R. Van Grieken, *Inorganic Mass Spectrometry*. Wiley Interscience, New York, USA and references therein (1988).
2. R. Geller, *Electron Cyclotron Resonance Ion Sources and ECR Plasmas*. IOP, Bristol, UK and references therein (1996).
3. P. Jardin, C. Barue, C. Canet, M. Dupuis, J.L. Flambard, G. Gaubert, N. Lecesne, P. Leherissier, F. Lemagnen, R. Leroy, J.-Y. Pacquet, F. Pellemoine, J.-P. Rataud, M.G. Saint Laurent and A.C.C. Villari, "Mono 1000: A simple and efficient 2.45 GHz electron cyclotron resonance ion source using a new magnetic structure concept", *Rev. Sci. Instrum.* **73,** 789 (2002). doi: 10.1063/1.1430869
4. M. Kidera, T. Nakagawa, K. Takahashi, S. Enomoto, R. Hirunuma, K. Igarashi, M. Fujimaki, E. Ikezawa, O. Kamigaito, M. Kase and Y. Yano, "Novel Technique for Trace Element Analysis using the ECRIS and Heavy Ion Linear Accelerator (ECRIS-AMS)", *AIP Conference Proceedings of the 16th International Workshop on ECR Ion Sources* **749,** 85 (2005). doi: 10.1063/1.1893372
5. Conference Proceedings of the *16th International Workshop on ECR Ion Sources AIP,* CA, USA **749,** and references therein (2005).
6. M. Imanaka, T. Kurita, M. Tukada, T. Nakagawa, M. Kidera, and S.M. Lee, "Effect of Magnetic Field Strength on Beam Intensity of Highly Charged Xe Ions from Liquid-He-Free Superconducting Electron Cyclotron Resonance Ion Source", *Japan. J. Appl. Phys.* **41,** 3926 (2002). doi: 10.1143/JJAP.41.3926
7. Ph. Collon, M. Bichler, J. Caggiano, L. DeWayne Cecil, Y. El Masri, R. Golser, C. L. Jiang, A. Heinz, D. Henderson, W. Kutschera, B.E. Lehmann, P. Leleux, H.H. Loosli, R. C. Pardo, M. Paul, K.E. Rehm, P. Schlosser, R.H. Scott, W.M. Smethie, Jr. and R. Vondrasek, "Development of an AMS method to study oceanic circulation characteristics using cosmogenic ^{39}Ar", *Nucl. Instrum. Methods* **B223,** 428 (2004). doi: 10.1016/j.nimb.2004.04.081
8. S. Niedermann and O. Eugster, "Noble gases in lunar anorthositic rocks 60018 and 65315: Acquisition of terrestrial krypton and xenon indicating an irreversible adsorption process", *Geochim. Cosmochim. Acta* **56,** 493 (1992). doi: 10.1016/0016-7037(92)90147-B
9. Y. Kawai, D. Meyer, A. Nadzeyka and K. Wiesemann, "Isotope effects in an electron cyclotron resonance ion source in mixtures of ^{15}N/^{14}N", *Plasma Sources Sci. Tech.* **10,** 451 (2001). doi: 10.1088/0963-0252/10/3/309
10. A.G. Drentje, A. Girard, D. Hitz and G. Melin, "Role of low charge state ions in electron cyclotron resonance ion source plasmas", *Rev. Sci. Instrum.* **71,** 623 (2000). doi: 10.1063/1.1150332
11. F.A. Podosek, J.C. Huneke, D.S. Burnett and G.J. Wasserburg, "Isotopic composition of xenon and krypton in the lunar soil and in the solar wind", *Earth Planet. Sci. Lett.* **10,** 199 (1971). doi: 10.1016/0012-821X(71)90008-2

Received: 26 October 2006
Revised: 26 September 2007
Accepted: 27 September 2007
Publication: 28 September 2007

Letter: New fragment ion production method using super cold electrons in electron cyclotron resonance plasma

Masanori Kidera, Kazuya Takahashi, Shuichi Enomoto, Akira Goto and Yasushige Yano
Nishina Center for Accelerator-Based Science, RIKEN, 2-1 Hirosawa, Wako, Saitama 351-0198, Japan. E-mail: kidera@kindex.riken.jp

We examined the fragmentation and ionization of molecules by low-temperature electrons generated by electron cyclotron resonance (ECR) plasma. We examined several types of metallocene compounds comprising a metal and 1,3-cyclopentadienes as ligands. We performed analyses using an ECR ion source (ECRIS) mass spectrometer. Consequently, we succeeded in ionizing fragments of an organometallic compound by adjusting the input power of the microwave introducing a super high-frequency plasma. Moreover, we succeeded in dynamically generating a significant quantity of fragment ions by continuously varying the input power. Information on the structure of a molecule may be acquired from this operation. Moreover, a molecule that could not be easily ionized thus far may now be ionizable when soft ionization is performed with this technique.

Keywords: electron cyclotron resonance, fragment, super cold electron, metallocene, ferrocene, nickelocene, osmocene, ECRIS mass spectrometer

Introduction

Devices that employ the electron cyclotron resonance (ECR) phenomenon are widely used in applications such as etching by plasma chemical vapor deposition (CVD), ion sputtering of devices and research on nuclear fusion reactors. An ECR ion source, particularly ECR ion sources used in heavy ion accelerators, is an ECR plasma device in which the plasma is confined in a characteristic magnetic field. Such ECR ion sources are of the minimum-B configuration developed by R. Geller *et al.* in 1960.[1] Since such ion sources confine electrons very well, the electron temperature can easily be increased and they can be used to supply an intense beam of highly-charged ions. On the other hand, since the electron confinement is very strong, even if the high-frequency input power for plasma production is quite low, the plasma is stably produced. We investigated this state in greater detail using our ion source[2] and the ECR plasma was generated by an input radio frequency (RF) power very as low as 55 mW.

In the case of electron ionization (EI), thermal electrons are used as the electron source and it is difficult to control low-temperature electrons with a high electron density; in contrast, the electron temperature can be controlled by varying the RF power in ECR ion sources. Moreover, due to the effect of electron confinement, it is expected that the collision rate will be greater than that in the EI method. This implies that the ionization efficiency will be good. The ionization efficiency is reported to exceed 40% in the case of He, Ne and Kr.[3] We have focused on the above-mentioned characteristics of ECR ion sources and examined the ionization with fragmentation for several metallocene compounds.

Ionization of molecules by using ECR plasma

First, we introduced nickelocene into the ECR plasma to examine the ionization of its molecules and to check the plasma status. When the plasma was not generated (i.e. the RF power is OFF), no ions were detected only by supplying an extraction voltage and feeding the evaporation gas of the organometallic compound. Next, when the RF power was increased gradually and it reached approximately 0.65 W, the plasma was generated. After the plasma was produced, even if the RF power was decreased gradually, the plasma was stably preserved. Figure 1 shows the variation in the

DOI: 10.1255/ejms.887 ISSN 1469-0667

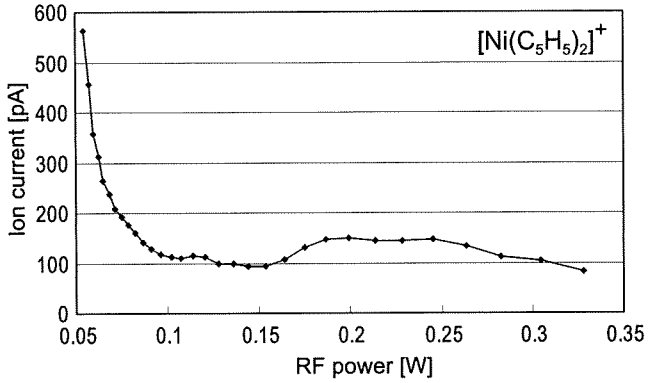

Figure 1. Nickelocene ion current as a function of the RF power.

peak current of the nickelocene ions with the RF power. As shown, an RF power of 54.7 mW is sufficient for the ion to be detected. This shows that the plasma is also generated at this RF power. Moreover, the emission of light of the ECR plasma has been visually checked in this state. Subsequently, when the RF power was adjusted to 50 mW, the plasma suddenly disappeared and nickelocene ions were not detected. Although the values of the RF power for the generation and disappearance of the plasma differed from the abovementioned value, similar tendencies were observed for other organometallic compounds (ferrocene and osmoceme) and their ions were detected. This value of RF power corresponded to that at the exit of a high-frequency amplifier (travelling wave tube amplifier: TWTA) and differed from the value at which the plasma was actually absorbed, which was lower. The electron temperature in the ECR plasma had a certain distribution that could be determined by careful measurements with a Langmuir probe and/or laser Thomson scattering measurement.[4]

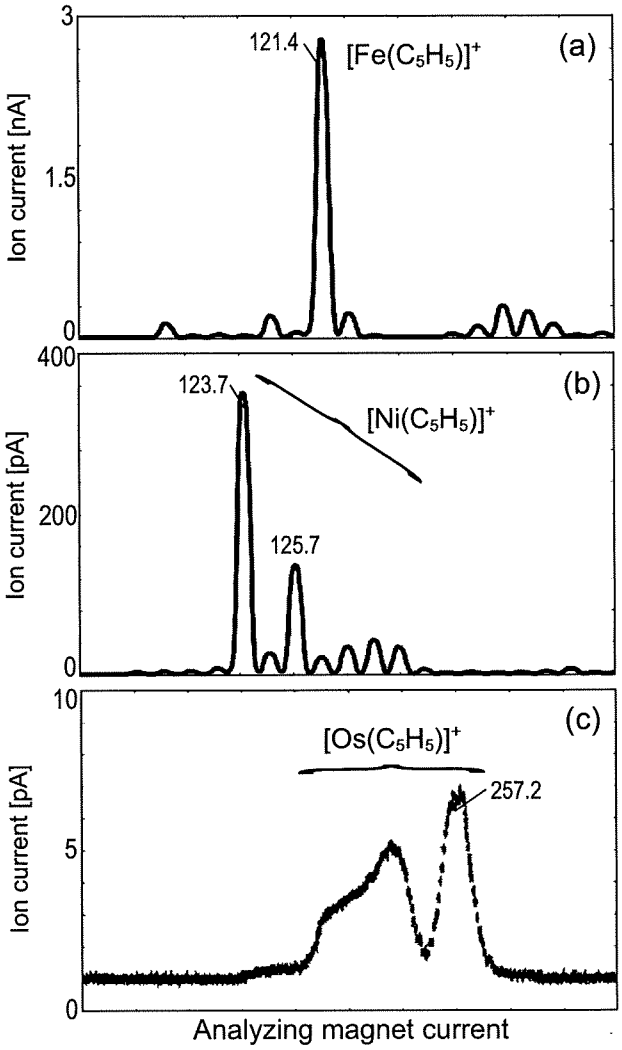

Figure 2. Spectrum of the fragment ions of the organometallic compounds.

Fragmentation and ionization control by varying RF power

Ferrocene, nickelocene and osmocene, which are organometallic compounds, were used for the ionization of a molecule and a fragment. These compounds have a structure wherein one metal element is sandwiched by two pentagons. These compounds have high vapor pressure at room temperature and, since these samples can be used in the form of gases, they are suitable for introducing a sample into the ECR ion source. The ECRIS mass spectrometer[2] was used for performing the analyses. The specifications of the ECR ion source can be obtained from Reference 2. Figures 2(a), (b) and (c) show the spectra of the fragment ions in which one pentagon is separated in each organometallic compound. This shows that ions can be stably generated from such chemically unstable fragments by using an ECR plasma. Figures 3(a), (b) and (c) show the variations in the maximum peak current corresponding to each spectrum of Figure 2 with the RF power. Since the RF power controls the electron temperature in the ECR plasma, the horizontal axis in Figure 3 can also be considered to represent the electron temperature. Since the electron temperature in the ECR plasma was controlled by varying the RF power, the generated quantity of the fragment ions was controlled.

Rough estimation of electron temperature

Here, we roughly estimate the mean electron temperature in the ECR plasma. In an ECR ion source, the electron confinement time (τ_e) usually increases with the electron temperature (T_e). For example, in the case of a minimum-B-type ECR ion source[1] that generates highly charged ions, τ_e is of the order of milliseconds. The transfer time (τ_t) for which energy is transferred from the RF power to a resonating electron is of the order of nanoseconds.[1] The electron traces a spiral orbit along magnetic lines of force and precesses

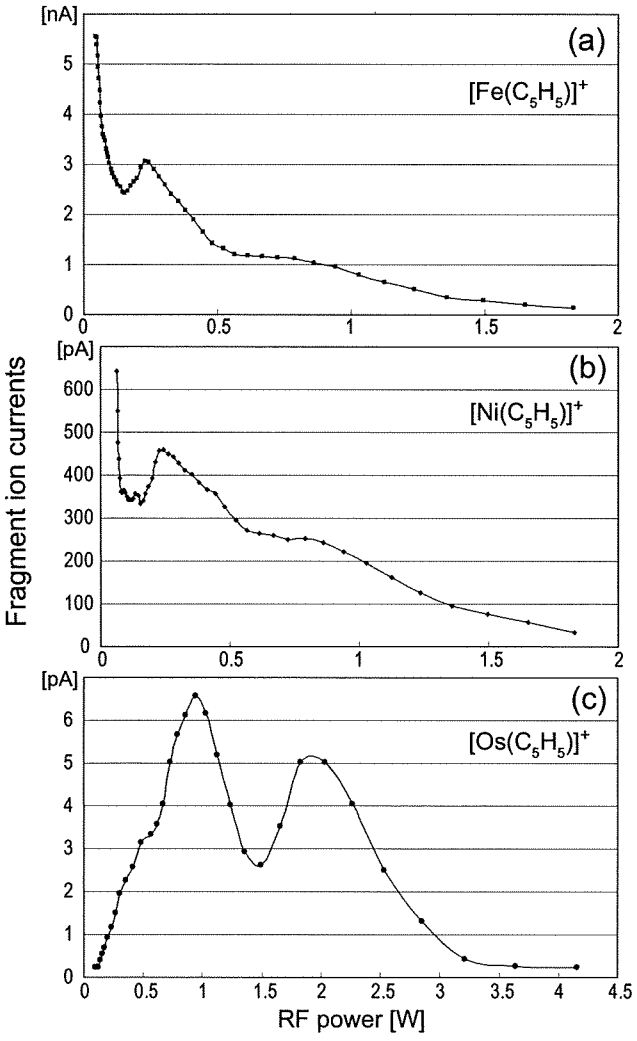

Figure 3. Fragment ion current of the organometallic compounds as a function of the RF power.

between the mirror magnetic fields. While the electron is confined by the mirror magnetic field, it passes along a resonating point repeatedly and energy is supplied to it from the RF power. On the other hand, τ_e becomes extremely small when T_e is very low. Here, when τ_e is very small (of the order of microseconds) and energy is supplied 1000 times (because τ_e and τ_i are of the order of microseconds and nanoseconds, respectively) at the resonating point during τ_e, the mean electron temperature $<T_e>$ is given as follows:

$$<T_e> \cong 1.602 \times 10^{19} \times 10^3 \times (C_a P_f \tau_i)(V_p n_e)^{-1} \text{ [eV]} \quad (1)$$

where C_a denotes the absorptivity coefficient of RF power; P_f [W], the input RF power; V_p [cm^3], the plasma volume; and n_e [cm^{-3}], the electron density. Here, by using typical values—$C_a = 0.7$,[5] $\tau_i = 10^{-9}$ s [1] and $V_p = 200$ cm^3—for an ECR ion source, we obtain the expression

$$<T_e> \cong 5.6 \times 10^{10} \times (P_f n_e^{-1}) \quad (2)$$

From Golovanivsky's diagram,[1] which is obtained by employing the step-by-step ionization criterion, the value of $n_e\tau_i$ optimized for the value of T_e that is required for (highly charged) ionization can be approximately estimated (τ_i is the ion confinement time). Here, we assume $n_e\tau_i = 10^6$ cm^{-3}·sec based on the extrapolation of the diagram since the ion in the plasma has mainly 1+; therefore, considering $\tau_i \cong \tau_e$, Equation (2) becomes

$$<T_e> \cong 5.6 \times 10^4 \times P_f \tau_e \quad (3)$$

$<T_e>$ caused by the RF power is shown in Figure 4 for a specific value of τ_e by using Equation (3). For example, when τ_e is 0.01 ms for an RF power of 55 mW, low-temperature electrons (super cold electrons) with a $<T_e>$ value of 31 meV will exist with a density of 10^{11} cm^{-3}. It is considered that the molecule ions and fragment ions (or fragmentation) are accomplished by such super cold electrons.

At electron temperatures of 1 eV or less, an electron–molecule collision involves a dominant momentum transfer process. However, the mechanism of fragmentation and fragment ionization in the ECR plasma is not well understood. It is expected that the mechanism will be clarified by future researches.

With regard to the plasma of the minimum-B-type ECR ion source, the plasma domain has not been researched extensively. Therefore, the above-mentioned estimates are rough approximations.

Summary

Organometallic compound molecules were soft-ionised by "super cold electrons" generated from an ECR plasma. Moreover, it was observed that the produced quantity of the fragment ions can be controlled by varying the RF power. Since the ionization of molecules and fragments by super cold electrons does not require a matrix, this ionization technique may potentially be used for the ionization of various chemical substances. Further, the dynamic control of the

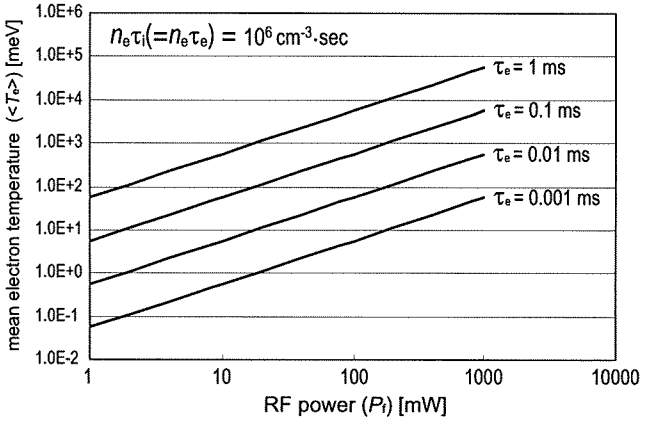

Figure 4. $<T_e>$ in the ECR plasma as a function of the RF power for τ_e = 1, 0.1, 0.01 and 0.001 ms.

fragmentation may potentially be used as a new method for the structural analysis (for example, from information on the strength of a chemical bond) of a chemical substance.

Acknowledgements

We are grateful to Mr M. Hemmi for assisting us with the microwave technique, electronics and ion current measurement. This study was supported by a Grant-in-Aid from the President's Discretionary Fund, RIKEN and a Grant-in-Aid for Scientific Research (KAKENHI: 19540515).

References

1. R. Geller, *Electron Cyclotron Resonance Ion Sources and ECR Plasmas.* IOP, Bristol, UK (1996) and references therein.
2. M. Kidera, K. Takahashi, S. Enomoto, Y. Mitsubori, A. Goto and Y. Yano, "Development of a novel mass spectrometer equipped with an electron cyclotron resonance ion source", *Eur. J. Mass Spectrom.* **13,** 239 (2007). doi: 10.1255/ejms.883
3. P. Jardin, C. Barue, C. Canet, M. Dupuis, J.L. Flambard, G. Gaubert, N. Lecesne, P. Leherissier, F. Lemagnen, R. Leroy, J.-Y. Pacquet, F. Pellemoine, J.-P. Rataud, M.G. Saint Laurent and A.C.C. Villari, "Mono 1000: A simple and efficient 2.45 GHz electron cyclotron resonance ion source using a new magnetic structure concept", *Rev. Sci. Instrum.* **73,** 789 (2002). doi: 10.1063/1.1430869
4. M.D. Bowden, T. Okamoto, F. Kimura, H. Muta, K. Uchino, K. Muraoka, T. Sakoda, M. Maeda, Y. Manabe, M. Kitagawa and T. Kimura, "Thomson scattering measurements of electron temperature and density in an electron cyclotron resonance plasma", *J. Appl. Phys.* **73,** 2732 (1993). doi: 10.1063/1.353046
5. Y. Higurashi, T. Nakagawa, M. Kidera, T. Aihara, M. Kase and Y. Yano, *Conference Proceedings of the 16th International Workshop on ECR Ion Sources,* No. 749. American Institute of Physics, California, USA p. 71 (2004).

Received: 28 September 2007
Revised: 29 October 2007
Accepted: 21 November 2007
Publication: 10 December 2007

DOI: 10.1007/s10967-007-0541-2 Journal of Radioanalytical and Nuclear Chemistry, Vol. 272, No.2 (2007) 429–431

Change of concentrations of trace elements and protein contents in the liver of zinc deficient mice

R. Minayoshi,[1]* T. Ohyama,[1,3] N. Kinugawa,[1] J. Kamishima,[1] T. Ogi,[1] K. Ishikawa,[2] M. Noguchi,[2] H. Suganuma,[1] K. Takahashi,[3] S. Enomoto,[3] M. Yanaga[1]

[1] Radiochemistry Research Laboratory, Faculty of Science, Shizuoka University, 836 Ohya, Suruga-ku, Shizuoka, 422-8529, Japan
[2] Department of Biology and Geosciences, Faculty of Science, Shizuoka University, 836 Ohya, Suruga-ku, Shizuoka, 422-8529, Japan
[3] Cyclotron Center, RIKEN (The Institute of Physical Chemical Research), 2-1, Hirosawa, Wako, Saitama 351-0198, Japan

(Received June 30, 2006)

The concentrations of essential trace elements and proteins in cytosolic fraction of hepatic cells of mice fed with Zn-deficient diet (Zn-def. mice) and control were determined by ICP-MS and BCA protein assay method, respectively, after division into forty fractions by gel filtration chromatography. The concentrations of zinc and proteins decreased in the 14–17th fractions of Zn-def. mice, whereas cobalt concentrations increased in the 14, 17, and 18th fractions. However, no significant differences were found on the gel after SDS-PAGE for the 12–21st fractions, although the BCA protein assay date showed the decrease of protein amounts in 13–15th fractions of Zn-def. mice.

Introduction

Zinc is one of the most important essential trace elements in living organisms, because of a variety of biochemical and physiological action. The zinc content in adult human is about 2.3 g.[1] This element is contained in detectable concentrations in skin, bone, liver, pancreas, kidney, and blood. It influences the activity of more than 300 enzymes that participate in a wide variety of metabolic processes, such as the metabolism and the synthesis of proteins and nucleic acid. A deficiency of zinc leads to various symptoms, such as growth retardation, hypogonadism, immunodeficient, alopecia, osteogenetic inhibition and so on.[2–4]

Previously, concentrations of zinc and other trace elements in various organs and tissues of Zn-def. mice were determined by means of instrumental neutron activation analysis (INAA).[5–7] The zinc concentrations in bone and pancreas of Zn-def. mice were significantly lower than those of control ones, although no differences were found in the other organs and tissues, such as liver, kidney and brain. On the other hand, concentrations of Co increased in all the organs and tissues of Zn-def. mice. Two works were carried out, in order to investigate the behavior of the metallic elements which bound proteins. One is the determination of the concentrations of trace elements and proteins after gel filtration chromatography for cytosolic fraction of hepatocytes. Another one is the investigation of affinities between metals and proteins which are contained in these fractions.

Experimental

Eighty 7-week old male mice of ICR strain were purchased from Clea Japan, Inc. (JCL), Tokyo, Japan, and fed with ordinary commercial diet and tap water. After a week, they were divided into two groups. One group was fed with Zn-deficient diet (<1 μg of Zn/g diet) and ultra pure water ad libitum (Zn-def. mice), and the other group fed with control diet (30 μg of Zn/g diet) and the same water as the former (control mice) ad libitum. The control diet consisted of raw materials for Zn-deficient diet and Zn as zinc carbonate, basic. Concentrations of minerals except for Zn in control diet were equal to those in Zn-deficient diet. After three weeks, their livers were removed and weighed, immediately. Then, every eight livers of each group was together homogenized and separated into two subcellular fractions, such as supernatant (cytosolic fraction) and the other fractions by ultracentrifugation. The cytosolic fraction, of 300 μl was loaded and was further divided into forty fractions (2 ml per a fraction) by gel filtration chromatography (Sephadex G-100 column, 1.5×70 cm^2) using Tris-HCl buffer (pH 7.4) as the eluent, at a flow rate of 10 ml/h, at 4 °C. Then, the concentration of the metallic elements and proteins in each fraction were determined by inductively coupled plasma mass spectrometry (ICP-MS) and BCA protein assay method, respectively. According to the results of ICP-MS, the 12–19th fractions in which the concentrations of zinc decreased were used for the following experiments. Proteins in these fractions were further separated with sodium dodecyl sulfate poly-achrylamide gel electrophoresis (SDS-PAGE).

* E-mail: r0432016@ipc.shizuoka.ac.jp

0236–5731/USD 20.00

Akadémiai Kiadó, Budapest
Springer, Dordrecht

Then, the gel was stained with silver stain. The affinities between trace elements and metalloproteins existing in the 14–16th fractions were examined by the multitracer technique.[8] Multitracer solution prepared from silver target was added to the fractions and incubated for 1 hour at 4 °C. Then, each solution was poured into several centrifugal filter tubes, such as Micron YM-3, -10, -30, and -50 (Millipore Co.), and centrifuged at 2000 *g* for 30 minutes in order to estimate the percentage of RI tracer bound to materials whose molecular weight are over 3, 10, 30, and 50 kDa, respectively. Radioactivities in those samples were measured with HPGe detectors. In each examination process, such as gel filtration chromatography, SDS-PAGE, and the multitracer experiment, the amounts of proteins in the samples for two groups were adjusted to be equal to each other.

The experiments were performed under the Guidelines for Animal Welfare and Experimentation of Faculty of Science, Shizuoka University.

Results and discussion

Figure 1 shows the concentrations of zinc and cobalt, determined by ICP-MS, in the 11–40th fractions of forty fractions divided by gel filtration chromatography for cytosolic fraction of hepatic cell. The concentrations of proteins in the same fractions were also shown in Fig. 2. The zinc concentrations in the 13–18, 21, and 22nd fractions of Zn-def. mice were much lower, and the cobalt concentrations in 14, 17, 18, 21, and 22nd fractions were higher than control ones as shown in Fig. 1. On the other hand, as shown in Fig. 2, the concentrations of proteins in 13–15th fractions of Zn-def. mice were low. These results indicate that some specific proteins in this region, especially in the 13–15th fractions, were related to a decrease in zinc and an increase in cobalt in Zn-def. mice. It is thought that the variations in the concentrations of zinc and cobalt were caused by changes to alternative states of proteins, such as liberation of metals from proteins, replacement of zinc in some specific proteins by cobalt and so on. Then, SDS-PAGE was performed in order to examine whether disappearance or induction of proteins occurred or not.

Typical results of the SDS-PAGE for the 14–17th fractions are shown in Fig. 3. No significant differences between Zn-def. and control mice were found on the positions and the number of the protein bands of the lanes on gel and also for the other fractions (12–21st).

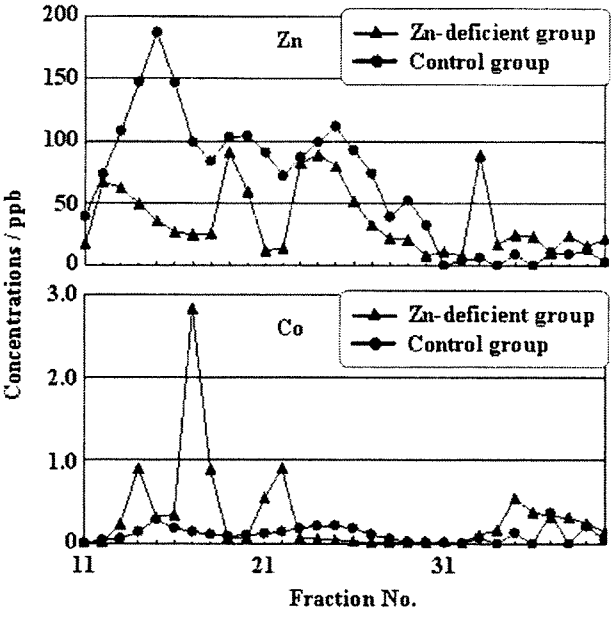

Fig. 1. Concentrations of zinc and cobalt after gel filtration chromatography for cytosolic fraction of hepatocytes in the 11–40th fractions

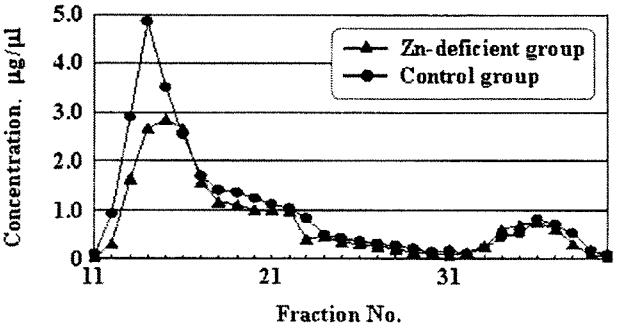

Fig. 2. Concentrations of proteins in the 11–40th fractions

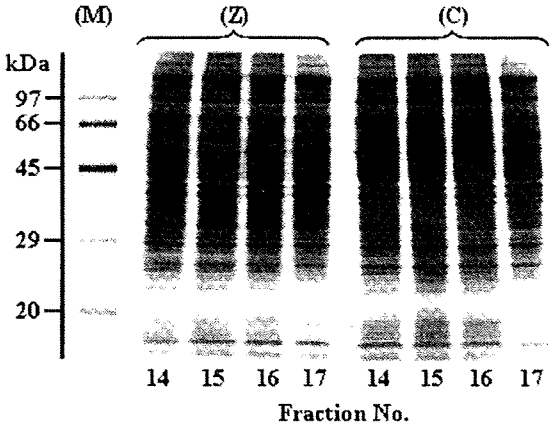

Fig. 3. Typical SDS-PAGE after silver staining for the 14–17th fractions; (M) protein marker, (Z) zinc-deficient mice, (C) control mice

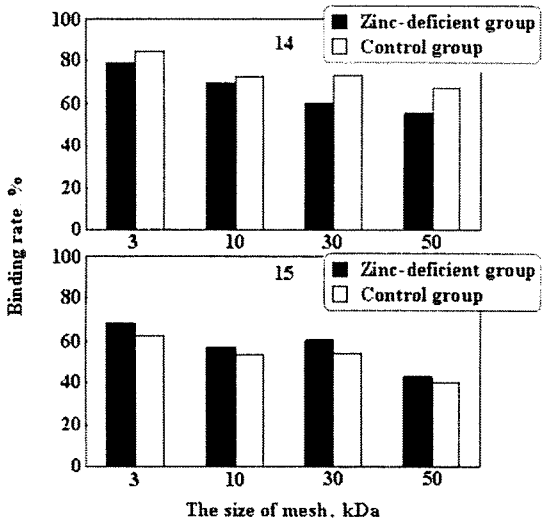

Fig. 4. Affinities between proteins and ^{65}Zn in the 14th and 15th fractions

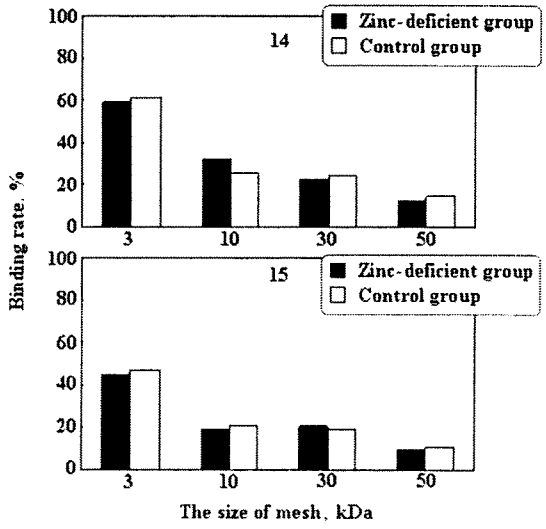

Fig. 5. Affinities between proteins and ^{56}Co in the 14th and 15th fractions

It might indicate that the possibilities of disappearance or a new appearance of proteins in the region of 17–116 kDa in these fractions are low. However, total amount of proteins in this region for the zinc deficient mice decreased as mentioned above.

The affinities between proteins and the radionuclides of ^{65}Zn, and ^{56}Co in the 14th and 15th fractions are shown in Figs 4 and 5, respectively. The affinities between ^{65}Zn and proteins over 30 kDa in the 14th fraction of Zn-def mice decreased, whereas the affinities to proteins over 10 kDa did not distinctly decrease. This result suggests that the zinc-binding proteins whose size is in a range of 10–30 kDa decreased or other metals replaced instead of zinc by zinc deficiency. On the other hand, as shown in Fig. 5, these were no differences between two groups on the affinities between ^{56}Co and proteins in the 14th and 15th fractions. Furthermore, the results in Fig. 5 also indicate that the size of cobalt affinitic proteins is almost in a range of 3–10 kDa. The direct evidence for the replacement of zinc with cobalt was not obtained by this carrier-free RI tracer examination for binding affinities. However, if it is considered that both elements of zinc and cobalt may be antagonistic[5–7] and also content of cobalt in organs is distinctly less than that of zinc, the enhancement of cobalt concentration in Zn-def. mice may be explained by substitution of zinc in some proteins with cobalt.

Conclusions

The concentrations of many essential trace elements and proteins of cytosolic fraction divided into forty fractions in Zn-def. mice were determined. The concentrations of zinc, cobalt, and proteins of Zn-def. mice were remarkably different from those of the control one. It indicates that zinc deficiency state leads to the change of the metalloproteins. The result of the multitracer experiments, affinities between ^{65}Zn and proteins in the 14th fraction, indicated that the zinc-binding proteins in a range of 10–30 kDa decreased or zinc was replaced by the other metal elements, whereas the results of SDS-PAGE showed that there were neither disappearance of metalloproteins nor induction of other proteins.

References

1. K. M. HAMBIDGE, C. E. SASEY, N. F. KREBS. Zinc, in: Trace Elements in Human and Animal Nutrition, Vol. 2, W. MERTZ (Ed.), Academic Press, San Diego, 1987, p. 1.
2. M. D. PESCOVITZ, P. L. JINDAL, M. L. MILGROM, S. B. LEAPMAN, R. S. FILO, Clin. Transplant., 10 (1996) 256.
3. D. CHEN, L. C. WAITE, W. M. PIERCE Jr., Biol. Trace Elem. Res., 68 (1999) 255.
4. M. C. CHA, A. ROJHANI, Biol. Trace Elem. Res., 59 (1997) 97.
5. M. YANAGA, M. IWAMA, K. TAKIGUCHI, M. NOGUCHI, T. OMORI, J. Radioanal. Nucl. Chem., 231 (1998) 187.
6. M. YANAGA, M. IWAMA, K. SHINOTSUKA, K. TAKIGUCHI, M. NOGUCHI, T. OMORI, J. Radioanal. Nucl. Chem., 243 (2000) 661.
7. M. YANAGA, H. WAKASA, T. YOSHIDA, M. IWAMA, K.SHINOTSUKA, M. NOGUCHI, T. OMORI, J. Radioanal. Nucl. Chem., 245 (2000) 255.
8. S. AMBE, S. Y. CHEN, Y. OHKUBO, Y. KOBAYASHI, M. IWAMOTO, M. YANOKURA, F. AMBE, Chem. Lett., (1991) 149.

Trace Nutrients Research 24 : 56 − 58 (2007)

牡蠣抽出物の胃液分泌能

五十嵐 香 織[1)], 金 山 洋 介[1)], 本 村 信 治[1)], 松 田 芳 和[2)], 榎 本 秀 一[1)]
([1)]理化学研究所*, [2)]日本クリニック株式会社**)

Effects of the Oyster Extract on the Gastric Secretion in Rats

Kaori IGARASHI[1)], Yosuke KANAYAMA[1)], Shinji MOTOMURA[1)],
Yoshikazu MATSUDA[2)] and Shuichi ENOMOTO[1)]
[1)]*Institute of Physical and Chemical Research (RIKEN),* [2)]*Japan Clinic Co., Ltd.*

Summary

Digestion is the process in which the bulk of ingested nutrients are broken down to oligomers or monomers in the mouth, stomach and intestine before they are absorbed and made available to all the cells of the body. Gastric juice is characterized by the presence of HCl, pepsin, mucus and an intrinsic factor. It is well established that the secretion of gastric juice is promoted by a type of amino acid and peptide. Oyster is a shellfish classified as Pelecypoda and is a nutritious food containing a great deal of zinc and taurine. Taurine has been reported to reduce myocardial damage and to have a beneficial effect on blood glucose and lipid levels. Thus, we investigated the effect of oyster extract on the gastric secretion in rats. Pylorus-ligated rats were sacrificed 6 h after the administration of oyster extract or taurine, and the gastric juice was collected and analyzed for volume, pH, acidity and pepsin activity. The results indicate that oyster extract may decrease pepsin activity and pepsin output; however, oyster extract significantly raised the acidity. Furthermore, it is suggested that the composition of oyster extract, excluding the taurine, may promote the secretion of HCl and organic acid because oyster extract more significantly raised acidity than taurine.

消化とは，摂取した食物を消化管内で吸収できる小分子の物質に変える働きであり，消化において，消化管の運動，消化液の生成，分泌およびその作用，腸粘膜における物質輸送は重要な要素である。

胃における消化は，食道から送り込まれた食塊を体温にまで温め，胃液含有物質により均質な液状に近い消化粥に変化させ，少量ずつ規則的に十二指腸へ送りこむことにより行われる[1)]。胃液は，胃の外分泌腺から分泌される種々の有機物質と無機電解質を含む液体であり，生理的に重要なのは，酸，ペプシン，粘液および内因子である[2)]。胃液の分泌は，ある種のアミノ酸およびペプチドにより促進されることが知られており[3)]，摂取する食物の含有成分が胃液分泌物やその量に影響をおよぼすことが推測される。

牡蠣は軟体動物斧足類に属する貝であり，必須微量元素のひとつである亜鉛などのミネラルを多く含む栄養食品として知られている。また，牡蠣は，心筋保護作用，血糖および血中コレステロール低下作用などを有する含硫アミノ酸であるタウリンを多く含んでいる[4,5)]。

そこで，我々は，牡蠣抽出物およびタウリンが胃液の分泌に及ぼす影響を検討するため，ラットを用いて胃液分泌実験を行った。

*所在地：埼玉県和光市広沢2-1（〒351-0198）
**所在地：京都府京都市右京区太秦開日町10-1（〒616-8555）

方　法

動物は，8週齢Wistar系雄性ラットを用いた。ラットの体重は209 ± 1.0 gであり，各群5匹とした。絶食後，エーテル麻酔下で開腹して幽門部を固く縛り，直ちに閉腹した[6]。その後，生理食塩水，牡蠣抽出物（日本クリニック株式会社製），タウリンをラットにゾンデにより経口投与した。牡蠣抽出物中のタウリン含有量は，5.4 g/100 gであり，投与溶液は，牡蠣抽出物138 mgを蒸留水で0.5 mLに調整したものとした。タウリンは，牡蠣抽出物溶液中タウリン含有量に相当する量を蒸留水で0.5 mLに調整した。試料投与6時間後にラットを解剖して胃を摘出し，内容物を採取して胃液量，ペプシン活性，ペプシン分泌量，酸度およびpHを測定した。ペプシン活性の測定にはAnson-Mirsky変法，胃液酸度の測定には滴定酸度測定法を用いた[7]。

結果および考察

生理食塩水，タウリンまたは牡蠣抽出物溶液を投与した場合におけるペプシン活性，ペプシン分泌量，胃液分泌量，酸度，pHをTable 1に示した。

タウリンを投与した群は，ペプシン活性がコントロール群に比べ有意に低値を示した。ペプシン分泌量，胃液分泌量およびpHではコントロール群に比べ低い傾向にあったが，有意な差は認められなかった。タウリン投与群の酸度は有意な差は認められなかったが，コントロール群に比べ高い傾向が認められた。これらのことから，タウリンは，ペプシン活性を低下させ，分泌量を低下させる可能性が示唆された。

牡蠣抽出物を投与した群におけるペプシン活性およびペプシン分泌量は，コントロール群およびタウリン投与群と比較し有意に低値を示した。胃液分泌量およびpHは，牡蠣抽出物投与群がコントロール群およびタウリン投与群に比べ低値であったが，有意な差は認められなかった。一方，牡蠣抽出物を投与した群における酸度は，コントロール群およびタウリン投与群と比較し有意に高値を示した。これらのことから，牡蠣抽出物は，タウリンに比べペプシン活性およびペプシン分泌量を低下させるが，酸度を上昇させることが示唆された。

本実験の結果から，タウリンは，ペプシン活性およびペプシン分泌量を低下させる傾向が認められた。一方，牡蠣抽出物は，ペプシン活性およびペプシン分泌量を抑制するが，胃液酸度を上昇させる可能性が示唆された。

胃酸は，胃液に含まれるタンパク質分解酵素であるペプシンの活性や作用を促進することにより間接的に消化に影響を及ぼす。牡蠣抽出物は，酸度を上昇させるにもかかわらずペプシンの活性および分泌量を低下させているが，消化におけるペプシンの作用が膵液の消化酵素により完全に代用されることから[2]，牡蠣抽出物投与によるペプシン活性および分泌量の低下は，消化に顕著な影響を及ぼさないことが推測された。本郷らは，胃酸分泌は，むしろ，膵外分泌機能を高める上で重要であると報告している[2]。胃酸は，十二指腸に到達すると粘膜の内分泌腺細胞を刺激し，セクレチンやコレシストキニンを分泌させる[2, 8]。セクレチンは，膵臓の導管細胞に作用して，Na^+，HCO_3^-の分泌を促進し，膵臓から分泌される消化酵素の活性を高める[2]。また，コレシストキニンは，セクレチンの作用を増強する[8]。本実験では，牡蠣抽出物投与時における膵液分泌の変化について検討は行っていないが，牡蠣抽出物が，上記の機構により膵液に含有される酵素活性を高める可能性が推測された。

また，牡蠣抽出物の酸度上昇作用は，タウリンに比べ顕著であったことから，牡蠣抽出物に含有されるタウリン以外

Table 1 Pepsin activity, pepsin output, volume, acidity and pH in the control, oyster extract- and taurine-administered rats

	Pepsin activity (μg/mL/min)	Pepsin output (trypsine μg)	Volume (mL)	Acidity (mEq/L)	pH
Control	1085 ± 149[a]	4079 ± 1531[a]	3.4 ± 0.9	38.4 ± 15.3[b]	4.2 ± 0.8
Oyster Extract	311 ± 65[c]	992 ± 290[b]	3.1 ± 0.3	119.4 ± 6.5[a]	3.6 ± 0.1
Taurine	725 ± 48[b]	2233 ± 570[a]	3.2 ± 0.9	49.0 ± 12.5[b]	3.8 ± 0.5

Values are means ± SE (n = 5). [a,b,c] Values with different superscript letters are significantly different ($p < 0.05$).

のアミノ酸またはペプチド等の影響である可能性が示唆された。Cieszkowskiらは，ポリペプチドおよび必須アミノ酸は胃酸分泌刺激物質であると報告している[9]。また，非必須アミノ酸であるアラニンは酸分泌を増加させるという報告もある[10]。本実験に用いた牡蠣抽出物には，必須アミノ酸，および比較的多くのアラニンが含まれることから，これらのアミノ酸の影響により，牡蠣抽出物投与時の酸度が上昇したと考えられた。

参考文献

1) 細谷憲政，武藤泰敏 (2002) 消化・吸収，第一出版，東京：pp. 50.
2) 本郷利憲，廣重　力，豊田順一 (2005) 標準生理学，医学書院，東京：pp. 690-691.
3) 細谷憲政，武藤泰敏 (2002) 消化・吸収，第一出版，東京：pp. 197.
4) Ueno T, Iguro Y, Yotsumoto G, Fukumoto Y, Nakamura K, Miyamoto TA, Sakata R (2007) Taurine at early reperfusion significantly reduces myocardial damage and preserves cardiac function in the isolated rat heart. Resuscitation 73(2): 287-295.
5) Tas S, Sarandol E, Ayvalik SZ, Serdar Z, Dirican M (2007) Vanadyl sulfate, taurine, and combined vanadyl sulfate and taurine treatments in diabetic rats: effects on the oxidative and antioxidative systems. Arch Med Res 38(3): 276-283.
6) Okabe S, Kunimi H (1981) Effects of N-acetyl-L-carnosine aluminum (CL-1700) on various acute gastric lesions and gastric secretion in rats. Japan J Pharmacol 31: 941-950.
7) 金井　泉，金井正光 (1993) 臨床検査法提要. 金原出版，東京：pp. 1313-1321.
8) 細谷憲政，武藤泰敏 (2002) 消化・吸収，第一出版，東京：pp. 202-203.
9) M Cieszkowski, SJ Konturek, W Obtulowicz, J Tasler (1974) Chemical stimulatory mechanism in gastric secretion. J Physiol 246: 143-157.
10) Ando M, Moriga M, Uchino H (1981) Effect of topical application of amino acids on gastric pepsin secretion in the rat. Gastroenterologia Japonica 16(2): 100-109.

J Neural Transm (2007) 114: 555–561
DOI 10.1007/s00702-006-0608-1
Printed in the Netherlands

Journal of Neural Transmission

Mental fatigue-induced decrease in levels of several plasma amino acids

K. Mizuno[1,2], M. Tanaka[1,2], S. Nozaki[1,2], K. Yamaguti[1,2], H. Mizuma[1], T. Sasabe[1,3], T. Sugino[4], T. Shirai[4], Y. Kataoka[1,2], Y. Kajimoto[4], H. Kuratsune[5], O. Kajimoto[4,6], Y. Watanabe[1,2]

[1] Department of Physiology, Osaka City University Graduate School of Medicine, Osaka, Japan
[2] The 21st Century COE Program "Base to Overcome Fatigue" (from the Ministry of Education, Culture, Sports, Science and Technology, the Japanese Government), Osaka, Japan
[3] Department of Oral Physiology, Osaka University Graduate School of Dentistry, Osaka, Japan
[4] Soiken Incorporation, Osaka, Japan
[5] Department of Health Science, Faculty of Health Science for Welfare, Kansai University of Welfare Sciences, Osaka, Japan
[6] Center for Health Care, Osaka University of Foreign Study, Osaka, Japan

Received: August 8, 2005 / Accepted: November 5, 2006 / Published online: December 11, 2006

Summary To investigate the relation between plasma amino acid levels and mental fatigue, we measured the plasma concentrations of 20 amino acids in 9 healthy volunteers before and after a fatigue-inducing mental task session for 8 hr. As fatigue-inducing mental tasks, the subjects performed an advanced trail making test, a Japanese KANA pick up test, and a mirror drawing test. As a control, 8-hr relaxation session was performed in the same subjects at an interval of 4 weeks. Immediately after the fatigue session, the plasma levels of branched-chain amino acids, tyrosine, cysteine, methionine, lysine, and arginine were below those after a relaxation session. The values for other blood parameters including total protein, albumin, glucose, and total cholesterol did not show any differences between the 2 sessions. These results indicate that mental fatigue may be characterized by a decrease in the plasma level of these amino acids.

Keywords: Mental fatigue, amino acids

Introduction

Fatigue is an everyday experience. However, in the case of chronic or accumulated fatigue, they affect the person's performance. In addition, long-term accumulated fatigue can lead to *Karoshi* (death as a result of overwork). For clinical use, mental fatigue is defined as difficulty in the initiation of, or the ability to, sustain voluntary activities (Chaudhuri and Behan, 2004). Mental fatigue, in contrast with neuromuscular or peripheral fatigue, represents a failure to complete mental tasks that require self-motivation and internal cues, in the absence of demonstrable cognitive failure or motor weakness (Chaudhuri and Behan, 2000). Based on this definition, Chaudhuri and Behan (2004) proposed a conceptual model for central fatigue. The work output of voluntary activity depends on the applied voluntary effort, which is controlled by motivational input and perceived effort via feedback from motor, sensory, and cognitive systems. Hence, any dissociation between the level of internal input (motivational and limbic) and that of the perceived effort from applied voluntary effort results in the sense of fatigue.

Physical fatigue can be derived from the action of the muscles, and is also known as peripheral fatigue. There are a large number of reports about the biochemical mechanisms of peripheral fatigue, e.g., depletion of glycogen and phosphocreatine, which are physical energy sources; a decrease in the resting membrane potential or dysfunction of the calcium pump in the sarcoplasmic reticulum in the skeletal muscles; and failure of neuromuscular transmission (For a review, see Fitts, 1994).

Several animal studies have shown that sustained exercise causes an increase in 5-HT turnover in some brain regions (Blomstrand et al., 1989; Chaouloff et al., 1989). Administration of a 5-HT agonist, *m*-chlorophenyl piperazine, to rats impaired running performance in a dose-dependent manner (Bailey et al., 1992) and that of a

Correspondence: Yasuyoshi Watanabe, MD, Department of Physiology, Osaka City University Graduate School of Medicine, 1-4-3 Asahimachi, Abeno-ku, Osaka 545-8585, Japan
e-mail: yywata@med.osaka-cu.ac.jp

5-HT antagonist, LY 53857, improved running performance (Bailey et al., 1993). These results suggest that this increased brain 5-HT level induced by sustained exercise is associated with physical fatigue. After exhaustive exercise, serum branched-chain amino acids (BCAA) levels were decreased by 22% from those before the exercise, whereas the level of free tryptophan in the serum increased by 74% (Lehmann et al., 1995). It has also been reported that plasma BCAA levels were decreased by 19%, whereas the plasma level of free tryptophan was increased by 15–17% after sustained exercise (Blomstrand et al., 1991). It is known that blood BCAA and free tryptophan compete for being transported into the brain through the blood-brain barrier, since they are carried by the same transport system (Pardridge, 1977). Thus, an increase in the ratio of plasma free tryptophan to BCAA accelerates the transport of free tryptophan into the brain; and thus, because tryptophan is a precursor of 5-HT, an increase in the 5-HT content in the brain may be expected. Therefore, plasma BCAA and free tryptophan levels are considered to be associated with physical fatigue.

Although the roles of amino acids in physical fatigue have to some extent been clarified, little is known about those in mental fatigue. From our preliminary experiments, it was not enough to evaluate the changes in plasma amino acid levels associated with fatigue by performing mental tasks for 4 hr. Therefore, in order to clarify the relationship between amino acids and mental fatigue, we evaluated changes in the level of all 20 plasma amino acids in healthy volunteers subjected to fatigue-inducing mental tasks for 8 hr.

Materials and methods

The study group consisted of 9 healthy volunteers [27.4 ± 5.2 years of age (mean ± SD), 4 females and 5 males]. The participants were recruited at Osaka City University. Current smokers, subjects having history of medical illness, taking chronic medication or supplemental vitamins, body weight less than 40 kg, having performed blood donation within one month before the study, or blood hemoglobin level less than 12.0 g/dl were excluded from the study. Good health was also assessed by physical examination, blood pressure, heart rate, blood chemistry panel (glucose, creatinine, uremic nitrogen, sodium, potassium, chloride, uric acid, and creatine phosphokinase), lipid profile (total cholesterol and triglyceride), complete blood count, and urinalysis. Furthermore, subjects who manifested psychiatric morbidity (e.g., depression) were excluded from the study. Psychiatric diagnosis was made by a psychiatrist (O. K.). The protocol was approved by the Ethics Committee of Kansai University of Welfare Sciences and all the subjects gave their written informed consent for the study.

All subjects underwent both fatigue and relaxation sessions. Four weeks after the relaxation session, the fatigue session was performed. Considering menstrual cycle for the female subjects, we conducted the fatigue session 4 weeks after the relaxation session. The day before either type of session, the subjects were instructed to avoid intensive physical and mental activities, to finish dinner by 10:00 p.m., and to fast overnight. At 9:00 a.m. on the following morning, the subjects recorded their subjective sensation of fatigue on a visual analogue scale (VAS) from 0 (no fatigue) to 100 (full exhaustion), and blood samples were collected. Thereafter, the subjects had breakfast (carbohydrate, 73.6 g; protein, 26.9 g; lipid, 32.3 g; total calories, 707 kcal) between 9:45 and 10:15 a.m. After breakfast either a relaxation or fatigue session was undertaken. As fatigue-inducing mental tasks, the subjects performed an advanced trail making test (Kajimoto et al., 2007) for 45 min, a Japanese KANA pick up test (Yamamoto, 1992) for 30 min, and a mirror drawing test (Yoshiuchi et al., 1997) for 45 min. These series of tasks began at 10:15 a.m., and 4 sessions of each series of tasks were performed, thus resulting in 8 hr of mental fatigue-inducing activities. After the end of the second series of tasks, the subjects had lunch (carbohydrate, 124.2 g; protein, 26.4 g; lipid, 16.3 g; total calories, 844 kcal) between 3:15 and 3:45 p.m. The time-interval between the first and second series of tasks and that between the third and fourth series were 30 min. After the end of the fourth series of the task, the subjects recorded again their subjective sensation of fatigue on the VAS, and blood samples were collected between 8:15 and 8:45 p.m. Then, they had dinner (carbohydrate, 126.3 g; protein, 23.4 g; lipid, 25.0 g; total calories, 882 kcal) between 8:45 and 9:15 p.m., and stayed at a hotel until the next morning. On the next morning at 7:30 a.m., the subjects recorded their subjective sensation of fatigue on the VAS, and blood samples were again collected. As for the relaxation sessions, the subjects read books, watched movies or chattered in the same time frame as the sessions for the mental tasks.

For the advanced trail-making test, the subjects performed visual search trials. In the test, circles numbered from 1 to 25 were first randomly located on the display of a personal computer. The subjects were required to touch these circles in sequence, starting with circle number 1. When the subjects touched the first target circle by using the computer mouse, it disappeared and circle number 26 appeared in a different position on the screen. The positions of the other circles remained the same. The subjects were required to memorize the positions of the other circles while searching for the target circle. This test is an advanced version of the conventional trail-making test (Reitan, 1955). They performed this test as quickly and as correctly as possible.

In the Japanese KANA pick up test, the subjects identified vowels in a novel as many and as correctly as possible. Every 8 min after the start of the test, the subjects were asked questions about the contents of the novel for 2 min.

In the mirror drawing test, the subjects traced a character on a hand glass mirror, which reversed the image. They performed this test as quickly and as correctly as possible.

Blood samples for the analysis of amino acids were collected from a brachial vein into a heparin-containing tube and kept on ice until centrifuged at 1700 *g* for 10 min at 4°C. The plasma sample was deproteinized with 5% trichloroacetic acid for 30 min on ice and centrifuged at 7500 *g* for 10 min at 4°C, after which the supernatant was stored at −80°C until analyzed. The concentration of amino acids in the supernatant was measured by using HPLC. Blood samples for the analysis of plasma glucose were collected in fluorosodium-containing tubes, and centrifuged at 1700 *g* for 10 min at 4°C. The supernatant of the plasma was stored at 4°C until analyzed. In the case of analysis of serum total protein, albumin, total cholesterol, high density lipoprotein cholesterol, triacylglycerol, creatine phosphokinase, and cortisol, the blood was allowed to coagulate at room temperature, and then the serum supernatants were obtained by centrifugation as described above and stored at −80°C until analyzed. All these assays were performed by the Special Reference Laboratories (SRL, Tokyo, Japan).

The values presented were shown as the mean ± SD unless otherwise stated. In order to exclude the influences of the confounding variables (such as diet, circadian rhythm, and gender) on the levels of plasma amino acids, we conducted the fatigue and relaxation sessions in the same time schedule and dietary contents, and compared just intra-individual differences across the sessions. Furthermore, in order to control for intra-individual variability of baseline values over the 4-week period that transpired between the 2

types of sessions, we determined baseline-adjusted net changes, which were the values obtained by subtracting those before the session from those after the session, as data for each time point (Ellenbogen et al., 1996). Comparisons between the 2 groups were performed by using 2-way analysis of variance (ANOVA) for repeated measures. When statistically significant effects were found, inter-group differences between the 2 groups were compared by using the paired *t*-test with Bonferroni correction. Statistical analyses were performed by using a Statview 5.0 software package (SAS Institute Inc., Cary, NC).

Results

Baseline characteristics of the various parameters before relaxation and fatigue sessions are summarized in Tables 1 and 2. Plasma cysteine and histidine levels before the fatigue session were significantly higher than those before the relaxation session. In the other parameters,

Table 1. *Various parameter levels before and after relaxation or fatigue session and the next morning*

	Before		8 hr		Next morning	
	Relaxation	Fatigue	Relaxation	Fatigue	Relaxation	Fatigue
VAS	36.8 ± 15.4	27.5 ± 17.5	42.4 ± 19.1	74.9 ± 16.2*	28.2 ± 13.0	44.2 ± 27.9
Total protein, g/l	80.6 ± 4.4	77.1 ± 4.0	76.7 ± 3.8	76.6 ± 4.2	76.8 ± 3.2	72.3 ± 2.9
Albumin, g/l	51.7 ± 3.0	49.3 ± 3.6	49.1 ± 1.9	48.6 ± 2.9	49.3 ± 3.0	45.4 ± 2.4
Plasma glucose, mmol/l	5.40 ± 0.39	5.21 ± 0.28	5.08 ± 0.54	4.96 ± 0.53	5.60 ± 0.25	5.43 ± 0.39
Total cholesterol, mmol/l	5.03 ± 0.69	5.05 ± 0.67	4.74 ± 0.63	4.98 ± 0.62	4.78 ± 0.58	4.69 ± 0.62
HDL cholesterol, mmol/l	1.77 ± 0.35	1.70 ± 0.44	1.66 ± 0.31	1.68 ± 0.33	1.65 ± 0.34	1.57 ± 0.32
Triacylglycerol, mmol/l	0.74 ± 0.47	0.87 ± 0.30	0.88 ± 0.63	0.90 ± 0.41	1.03 ± 0.57	1.05 ± 0.54
Creatine phosphokinase, IU/l	98.2 ± 38.6	109.8 ± 79.4	92.4 ± 37.6	97.7 ± 61.7	114.8 ± 72.9	99.9 ± 60.4
Cortisol, nmol/l	346.7 ± 119.5	308.1 ± 105.9	192.8 ± 150.3	136.4 ± 37.7	436.8 ± 146.6	413.9 ± 101.3

VAS Visual analogue scale; *HDL* high density lipoprotein.
Data are presented as the mean ± SD.
* $P < 0.05$, significantly different from the corresponding values of the relaxation session (2-way ANOVA for repeated measures, followed by paired *t*-test with Bonferroni correction).

Table 2. *Plasma amino acid levels before and after relaxation or fatigue session and the next morning*

	Before		8 hr		Next morning	
	Relaxation	Fatigue	Relaxation	Fatigue	Relaxation	Fatigue
Valine, μmol/l	213.1 ± 47.9	225.2 ± 44.5	275.8 ± 45.8	242.6 ± 36.0	237.6 ± 34.4	233.5 ± 26.9
Leucine, μmol/l	106.4 ± 25.5	119.3 ± 25.9	154.3 ± 35.1	116.0 ± 21.8[a]	126.6 ± 21.7	121.7 ± 17.6
Isoleucine, μmol/l	59.0 ± 14.8	63.2 ± 15.2	95.9 ± 21.8	72.6 ± 15.5[c]	78.6 ± 14.2	73.9 ± 11.2
BCAA, μmol/l	378.4 ± 86.5	407.7 ± 82.0	525.9 ± 101.0	431.2 ± 69.9[c]	442.8 ± 67.3	429.1 ± 52.1
Tyrosine, μmol/l	53.5 ± 7.5	57.7 ± 7.5	69.7 ± 9.3	55.3 ± 5.8[a]	66.6 ± 11.4	67.6 ± 9.0
Phenylalanine, μmol/l	53.8 ± 5.3	56.2 ± 6.6	68.2 ± 8.1	60.7 ± 3.8	59.5 ± 4.8	55.6 ± 5.2
Tryptophan, μmol/l	60.6 ± 12.5	59.8 ± 9.6	70.0 ± 14.2	54.9 ± 9.4	64.1 ± 14.5	57.5 ± 9.8
Cysteine, μmol/l	30.6 ± 3.8	40.5 ± 4.3[a]	33.7 ± 4.6	36.7 ± 4.2[c]	38.1 ± 4.0	38.5 ± 4.8
Methionine, μmol/l	24.0 ± 3.1	28.0 ± 4.7	38.6 ± 9.0	26.2 ± 5.7[b]	30.1 ± 5.3	28.6 ± 3.1
Lysine, μmol/l	167.5 ± 26.0	189.3 ± 31.3	231.7 ± 48.9	192.1 ± 34.9	194.5 ± 33.3	174.0 ± 18.2
Arginine, μmol/l	69.5 ± 16.6	76.5 ± 14.6	107.7 ± 23.2	84.1 ± 17.4	86.0 ± 12.9	81.9 ± 14.3
Histidine, μmol/l	71.2 ± 8.7	79.0 ± 9.8[a]	80.1 ± 11.4	79.6 ± 9.4	76.3 ± 8.7	74.2 ± 7.6
Serine, μmol/l	117.1 ± 24.7	112.7 ± 15.5	127.1 ± 30.3	113.6 ± 25.9	124.7 ± 30.2	117.7 ± 22.6
Threonine, μmol/l	127.5 ± 17.6	130.0 ± 24.5	144.7 ± 24.9	124.0 ± 26.0	146.8 ± 29.1	133.9 ± 20.1
Asparagine, μmol/l	43.1 ± 5.2	47.0 ± 4.2	54.2 ± 6.8	52.8 ± 9.2	49.4 ± 7.2	49.2 ± 6.5
Aspartate, μmol/l	N.D.	N.D.	N.D.	N.D.	N.D.	N.D.
Glutamine, μmol/l	567.9 ± 63.3	536.9 ± 76.1	631.4 ± 83.1	557.5 ± 88.4	607.5 ± 79.5	526.4 ± 60.8
Glutamate, μmol/l	30.0 ± 12.0	33.3 ± 10.7	29.6 ± 13.8	30.6 ± 12.9	33.3 ± 12.2	38.2 ± 13.8
Glycine, μmol/l	222.7 ± 67.7	229.5 ± 56.3	255.0 ± 70.1	245.2 ± 78.9	247.4 ± 69.8	248.8 ± 67.1
Alanine, μmol/l	299.1 ± 53.1	302.2 ± 58.8	375.1 ± 43.9	335.8 ± 46.4	332.5 ± 47.0	342.7 ± 70.2
Proline, μmol/l	139.8 ± 35.9	124.7 ± 29.4	172.1 ± 27.4	147.9 ± 26.9	153.9 ± 13.9	144.4 ± 23.2

BCAA Branched-chain amino acids (total for valine, leucine, and isoleucine); *N.D.* not detected.
Data are presented as the mean ± SD.
[a] $P < 0.05$, [b] $P < 0.01$ significantly different from the corresponding values of the relaxation session (2-way ANOVA for repeated measures, followed by paired *t*-test with Bonferroni correction).
[c] $P < 0.1$, different from the corresponding values of the relaxation session (2-way ANOVA for repeated measures, followed by paired *t*-test with Bonferroni correction).